

## Article

# Numerical and Experimental Analysis of the ZFC Heat Release from a YBCO Bulk and Validation of YBCO Thermal Parameters

António J. Arsénio Costa <sup>1,\*</sup>, João F. P. Fernandes <sup>1,2</sup>, Rui Melicio <sup>1</sup>, Carlos Cardeira <sup>1,2</sup>  
and Paulo J. Costa Branco <sup>1,2</sup>

<sup>1</sup> Instituto de Engenharia Mecânica (IDMEC), Laboratório Associado de Energia Transportes e Aeronáutica (LAETA), Av. Rovisco Pais, 1, 1049-001 Lisboa, Portugal

<sup>2</sup> IDMEC, Instituto Superior Técnico (IST), Universidade Lisboa (UL), Av. Rovisco Pais, 1, 1049-001 Lisboa, Portugal

\* Correspondence: antoniojcosta@tecnico.ulisboa.pt

**Abstract:** This article presents results from a simple experimental methodology used to determine the amount of heat transferred from an yttrium barium copper oxide (YBCO) bulk to liquid nitrogen (LN<sub>2</sub>) and LN<sub>2</sub> consumption during the process of zero-field cooling (ZFC). The thermal power can be determined from the YBCO bulk temperature variation, which is difficult to measure with accuracy. In this procedure, the thermal power from the YBCO bulk to LN<sub>2</sub> is determined from the measured rate of LN<sub>2</sub> evaporation, considering the LN<sub>2</sub> latent heat. To reduce the influence of room temperature heating and make the LN<sub>2</sub> mass variation depend as much as possible on the heat released from the YBCO bulk, a step transient from room temperature into the LN<sub>2</sub> is performed. The precision of results is determined from the rate of LN<sub>2</sub> evaporation due to room temperature heating with the bulk already cooled by ZFC. The temperature evolution at the bulk lateral surface where the heat transfer is higher is also measured. The results from experimental measurements are compared with 3D finite element analysis (FEA) numerical results. The obtained evolutions of the temperature and thermal power from the YBCO bulk are used to validate YBCO thermal parameters, such as thermal conductivity and specific heat capacity at constant pressure. The YBCO bulk equivalent heat capacity and thermal resistance are determined by analyzing the equivalent first-order thermal lumped parameter circuit based on the obtained evolutions in time of the YBCO temperature and heat transferred to the LN<sub>2</sub>. The characteristics of dependence of the YBCO thermal resistance and heat capacity with temperature are obtained by correlating their time evolutions with the bulk average temperature evolution in time. The YBCO-specific heat capacity at constant pressure is then calculated by dividing the obtained bulk heat capacity by the bulk mass. The YBCO thermal conductivity is calculated from the obtained thermal resistance considering an equivalent bulk section and length toward the main direction of heat flux.

**Keywords:** YBCO bulk; zero-field cooling; LN<sub>2</sub> evaporation; latent heat; thermal lumped parameter circuit; first-order step response; thermal conductivity; specific heat capacity



**Citation:** Arsénio Costa, A.J.; Fernandes, J.F.P.; Melicio, R.; Cardeira, C.; Costa Branco, P.J. Numerical and Experimental Analysis of the ZFC Heat Release from a YBCO Bulk and Validation of YBCO Thermal Parameters. *Crystals* **2023**, *13*, 532. <https://doi.org/10.3390/cryst13030532>

Academic Editors: Hongye Zhang and Kévin Berger

Received: 29 December 2022

Revised: 25 February 2023

Accepted: 15 March 2023

Published: 20 March 2023



**Copyright:** © 2023 by the authors. Licensee MDPI, Basel, Switzerland. This article is an open access article distributed under the terms and conditions of the Creative Commons Attribution (CC BY) license (<https://creativecommons.org/licenses/by/4.0/>).

## 1. Introduction

The main objective of this article is to present the results from a simple experimental methodology used to easily determine the amount of heat released specifically by an yttrium barium copper oxide (YBCO) bulk and associated LN<sub>2</sub> consumption during its zero-field cooling (ZFC). This amount of heat is independent of the cooling process's duration and related to the amount of thermal energy change in the bulk mass. The thermal power can be determined from the YBCO bulk average temperature variation, which is difficult to measure with accuracy. The adopted methodology consists of determining the thermal power from the measured LN<sub>2</sub> mass loss rate in the liquid-to-gas phase change (evaporation) after a step transition of the bulk from room temperature down to the

LN<sub>2</sub> temperature. Such stepped temperature transition minimizes the influence of room temperature heating, and the LN<sub>2</sub> mass variation depends almost on the heat released from the YBCO bulk. The precision of results is determined from the rate of LN<sub>2</sub> evaporation due to room temperature heating with the bulk already cooled by ZFC. The presented experimental methodology allows us to easily determine with expected precision the heat released from YBCO bulks during their ZFC, which is independent of the cooling process's duration and related to the amount of thermal energy change in the bulk mass.

Another objective is to validate the YBCO thermal parameters, such as thermal conductivity and specific heat at constant pressure. YBCO bulks are defined by a specific thermal resistance and heat capacity, and their interaction with the environment temperature is defined by a first-order system. The YBCO bulk thermal resistance and heat capacity are determined by analyzing the first-order step response evolutions of the YBCO bulk average temperature and thermal power from the YBCO bulk to the LN<sub>2</sub>. The characteristics of dependence of the YBCO thermal resistance and heat capacity with temperature are obtained by correlating their time evolutions with the bulk average temperature evolution in time. The YBCO thermal conductivity is obtained from the bulk thermal resistance considering the equivalent bulk length and area toward the main direction of heat flux. The YBCO-specific heat capacity at constant pressure is obtained by dividing the bulk heat capacity by its mass.

The cooling of YBCO bulks should be accomplished slowly and progressively and not in direct contact with the liquid nitrogen (LN<sub>2</sub>) [1]. This is to reduce the applied thermal stress and avoid bulk cracking [2,3]. YBCO bulks should not be in direct contact with LN<sub>2</sub> so they can be kept dry [3]. Typical LN<sub>2</sub> cryostat structures for high-temperature superconductor (HTS) bulks are presented and described in [4–10]. In the presented structures, HTS bulks are not in direct contact with LN<sub>2</sub> and the heat is transferred to the LN<sub>2</sub> via a material presenting high thermal conductivity. Usually, copper is used as the high thermal-conduction medium. Not only the HTS bulks but also the material presenting high thermal conductivity are cooled, and the released heat comes from both materials. Because of this reason and because the cooling of HTS bulks in cryostats occurs progressively, it is difficult to accurately measure the bulk average temperature evolution and, from this estimate, the heat released from HTS bulks during their ZFC in cryostats.

Results from experimental measurements are validated by 3D finite element analysis (FEA). The thermo-fluid models considered in the 3D FEA are described in Section 2. A preliminary study to predict heat flux and LN<sub>2</sub> consumption using 2D axisymmetric FEA was performed [11]. The methodology used to calculate the released thermal power evolution from the measured LN<sub>2</sub> mass loss rate is described in Section 3. This methodology was used to analyze the autonomous safety service time of a horizontal HTS ZFC levitating bearing [12]. The geometry of such a bearing was optimized in [13] for the maximization of its guiding stability. Experimental and 3D FEA numerical analyses of the YBCO temperature and heat release evolutions are performed in Section 4. The calculations of the characteristics of YBCO thermal conductivity and specific heat capacity at constant pressure from the measured step responses of temperature and heat transfer are performed in Section 5. In conclusion, the main results are presented and discussed in Section 6.

## 2. Thermo-Fluid Models and Parameters

### 2.1. Heat Transfer Modeling

The phenomena of heat transfer by convection-diffusion [14,15] are expressed by the partial differential (PDE) Equation (1),

$$\rho C_p \frac{\partial T}{\partial t} + \rho C_p \mathbf{u} \cdot \nabla T - k \nabla^2 T = Q \quad (1)$$

where  $T$  is the absolute temperature,  $\mathbf{u}$  is the velocity,  $\rho$  is the volumetric density,  $k$  is the thermal conductivity,  $C_p$  is the specific heat capacity at constant pressure, and  $Q$  is the heating source volumetric power density. The latter can express, for example, the

volumetric power density of Joule losses in superconductor domains. The thermal power flux  $q$  is given according to Fourier’s law (2).

$$q = k \nabla T \tag{2}$$

Table 1 presents the values and characteristics of  $\rho$ ,  $k$ , and  $C_p$  in the literature for the materials used in the experiments: YBCO [16–20], extruded polystyrene (XPS) and polyurethane (PUR) foams [21,22], LN<sub>2</sub> [23–25], N<sub>2</sub> [25,26], and air [26]. Equations (3) and (4) correspond to models for the dependence on the temperature of the YBCO thermal conductivity and specific heat capacity at constant pressure. These two characteristics are plotted in Figure 1. Equation (5) gives the characteristic of LN<sub>2</sub> thermal conductivity dependence on temperature.

**Table 1.** Values and characteristics considered for  $\rho$ ,  $k$ , and  $C_p$ .

Medium	$\rho$ [kg m <sup>-3</sup> ]	$k$ [W m <sup>-1</sup> K <sup>-1</sup> ]	$C_p$ [J kg <sup>-1</sup> K <sup>-1</sup> ]
YBCO [16–20]	5900	(3)	(4)
XPS foam [21,22]	30	0.03	1350
PUR foam [21,22]	40	0.025	1400
LN <sub>2</sub> [23–25]	808.5	(5)	2042
Air [26]	1.25	0.025	1005

$$k_{YBCO} = \begin{cases} 6.92 + 0.35T + 3.31 \times 10^{-3}T^2 - 1.68 \times 10^{-4}T^3 + 1 \times 10^{-6}T^4 & ; & 0 \text{ K} \leq T \leq 77 \text{ K} \\ 11.9 + 0.004 T & ; & 77 \text{ K} < T \leq 300 \text{ K} \end{cases} \tag{3}$$

$$C_{PYBCO} = \begin{cases} 38.76 + 1.46 T & ; & 0 \text{ K} \leq T \leq 230 \text{ K} \\ -23.1 + 2.8 T - 5.6 \times 10^{-3} T^2 + 4.1 \times 10^{-6}T^3 & ; & 230 \text{ K} \leq T \leq 300 \text{ K} \end{cases} \tag{4}$$

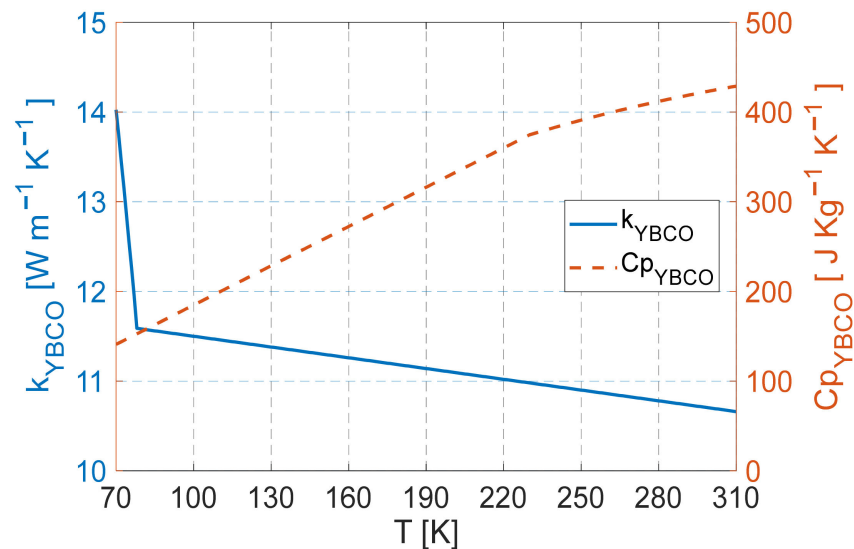


**Figure 1.** Characteristics of  $k_{YBCO}$  and  $C_{PYBCO}$  with temperature from the literature.

$$k_{LN_2} = \begin{cases} 0.275 - 1.791 \times 10^{-3} T & ; & 63 \text{ K} \leq T \leq 145 \text{ K} \\ 1 \times 10^{-3} + 7.38 \times 10^{-5} T + 1.51 \times 10^{-7} T^2 - 5.54 \times 10^{-10}T^3 & & \\ +5.21 \times 10^{-13}T^4 & ; & 145 \text{ K} < T \leq 300 \text{ K} \end{cases} \tag{5}$$

The internal boundaries (between YBCO and LN<sub>2</sub> and between LN<sub>2</sub> and the foam walls) are considered continuities of the normal component of thermal power flux  $q$ , expressed by the Neumann boundary condition in Equation (6),

$$\partial q / \partial n = 0 \quad (6)$$

where  $n$  is the unit length vector, normal to the considered internal boundary.

For the external boundaries in direct contact with the air, one considers the transfer of heat flux  $q_e$  by natural convection from the air, with the magnitude given by Equation (7),

$$q_e = h (T_e - T) \quad (7)$$

where  $h$  is the convection coefficient that depends on the characteristics of the external boundary surface and  $T_e$  is the external room temperature far from that surface. According to [15], the coefficients of free convection to the air through horizontal and vertical surfaces are estimated using Equations (8) and (9), respectively.

$$h_h = \frac{k}{L} 0.54 R_a^{\frac{1}{4}} \quad (8)$$

$$h_v = \frac{k}{L} \left( 0.68 + \frac{0.67 R_a^{\frac{1}{4}}}{\left[ 1 + \left( \frac{0.492 k}{\mu C_p} \right)^{\frac{9}{16}} \right]^{\frac{4}{9}}} \right) \quad (9)$$

where  $k$  and  $C_p$  are the thermal conductivity and heat capacity of the air, respectively, with typical values given in Table 1 and  $\mu$  is the dynamic viscosity of air with a value of about  $20 \times 10^{-6}$  Pa s at 1 atm [26]. The Rayleigh number  $R_a$  assumes a value of  $10^7$  in the case of free convection to the air [16]. The parameter  $L$  is a linear dimension given by the ratio between the horizontal area and perimeter in Equation (8) and the vertical wall height in Equation (9). For the boundaries with LN<sub>2</sub>, where heat transfer causes a phase change of LN<sub>2</sub>, the rate of LN<sub>2</sub> evaporated mass flux is given by Equation (10),

$$\Phi_{mLN2} = q / L_{LN2} \quad (10)$$

where  $q$  is the magnitude of heat flux through those boundaries and  $L_{LN2}$  is the latent heat of LN<sub>2</sub> assuming  $199 \text{ J g}^{-1}$  [23–25].

## 2.2. Fluid-Flow Modeling

The flow of Newtonian incompressible fluids [27,28] is expressed by the Navier–Stokes momentum PDE Equation (11),

$$\rho \frac{\partial \mathbf{u}}{\partial t} + \rho \mathbf{u} \cdot \nabla \mathbf{u} - \mu \nabla^2 \mathbf{u} = -\nabla p + \rho \mathbf{g} \quad (11)$$

where  $\mathbf{u}$  is the velocity,  $p$  is the pressure,  $\rho$  is the fluid volumetric density, and  $\mu$  is the dynamic fluid viscosity. LN<sub>2</sub> has a dynamic viscosity  $\mu_{LN2}$  of about  $152 \times 10^{-6}$  Pa s at 1 atm [23–25], and air has a dynamic viscosity  $\mu_{air}$  of about  $20 \times 10^{-6}$  Pa s at 1 atm [26].

In the case of the continuity of mass, Equation (12) is verified.

$$\frac{\partial \rho}{\partial t} + \rho \nabla \cdot \mathbf{u} = 0 \quad (12)$$

In the case of incompressible fluids, there is no variation in the fluid density with time (Equation (13)).

$$\frac{\partial \rho}{\partial t} = 0 \quad \langle \Rightarrow \rangle \quad \nabla \cdot \mathbf{u} = 0 \quad (13)$$

For boundaries between fluids and solid domains, the Dirichlet condition, in which the fluid velocity normal component is zero, is applied.

$$\mathbf{u}_n = 0 \quad (14)$$

For boundaries between fluids, the continuity of the pressure normal component is expressed by the Neumann boundary condition (Equation (15)), where  $n$  is the unit length vector normal to those boundaries.

$$\partial p / \partial n = 0 \quad (15)$$

The evaluation of the laminar or turbulent regime is performed by estimating the Reynolds number  $R_e$  given by Equation (16).

$$R_e = \frac{\rho \bar{u} L}{\mu} \quad (16)$$

where  $\bar{u}$  is the average value of the flow velocity concerning an object and  $L$  is a linear dimension defined by the relation between the volume of that object and the effective object section normal to  $u$ . Turbulent regimes occur for  $R_e$  greater than  $4 \times 10^3$  [27,28].

In a turbulent regime, the fluid velocity  $u$  results from the sum of the mean velocity  $\bar{u}$  and the turbulent velocity term  $u'$ .

$$u = \bar{u} + u' \quad (17)$$

Additionally, the fluid pressure  $p$  results from the sum of the mean pressure  $\bar{p}$  and the turbulent pressure  $p'$ .

$$p = \bar{p} + p' \quad (18)$$

The standard  $\kappa - \varepsilon$  turbulence model, which is derived from the Reynolds-averaged Navier–Stokes (RANS) equations [28], is adopted to simulate turbulent regimes. According to [29], the two governing equations of the standard RANS  $\kappa - \varepsilon$  model are Equations (19) and (20).

$$\rho \frac{\partial \kappa}{\partial t} + \rho \bar{u} \cdot \nabla \kappa = \nabla \cdot \left( \frac{\mu_t}{\sigma_\kappa} \nabla \kappa \right) + P_k - \rho \varepsilon \quad (19)$$

$$\rho \frac{\partial \varepsilon}{\partial t} + \rho \bar{u} \cdot \nabla \varepsilon = \nabla \cdot \left( \frac{\mu_t}{\sigma_\varepsilon} \nabla \varepsilon \right) + C_{\varepsilon 1} \frac{\varepsilon}{\kappa} P_k - C_{\varepsilon 2} \rho \frac{\varepsilon^2}{\kappa} \quad (20)$$

In this model,  $\kappa$  is the turbulent kinetic energy, and  $\varepsilon$  the rate of dissipation of turbulent energy, which are calculated according to Equations (21) and (22), respectively:

$$\kappa = \frac{u' \cdot u'}{2} = \frac{1}{2} \sum_i (u'_i)^2 \quad (21)$$

$$\varepsilon = \frac{\nu}{2} \sum_{i \neq j} \left( \frac{\partial u'_i}{\partial x_j} + \frac{\partial u'_j}{\partial x_i} \right)^2 \quad (22)$$

where  $u'_i$  is, according to Einstein's notation, the intensity of the fluid's turbulent velocity according to the space dimension  $x_i$  and  $\nu$  the fluid kinetic viscosity given by Equation (23).

$$\nu = \frac{\mu}{\rho} \quad (23)$$

Variable  $\mu_t$  is the turbulent or Eddy viscosity calculated by Equation (24).

$$\mu_t = \rho C_\mu \frac{\kappa^2}{\varepsilon} \quad (24)$$

Variable  $P_k$  is the rate of production of turbulent kinetic energy calculated by Equation (25),

$$P_k = \frac{1}{2} \mu_t \sum_{i \neq j} \left( \frac{\partial \bar{u}_i}{\partial x_j} + \frac{\partial \bar{u}_j}{\partial x_i} \right)^2 \quad (25)$$

where  $\bar{u}_i$  is the intensity of fluid mean velocity according to the space dimension  $x_i$ .

A typical value for  $C_\mu$  is 0.09,  $C_{\varepsilon 1}$  is 1.44,  $C_{\varepsilon 2}$  is 1.92,  $\sigma_\kappa$  is 1.0, and  $\sigma_\varepsilon$  is 1.3, which are all adopted for the five parameters of the standard RANS  $\kappa - \varepsilon$  model [29].

### 3. Methodology to Estimate Thermal Power from the LN<sub>2</sub> Evaporation Rate

The thermal power associated with the variation in the YBCO bulk internal energy  $U_{SC}$  can be determined from the measured evolution of the YBCO bulk average temperature  $\bar{T}_{SC}$  by Equation (26),

$$P_{t SC} = \partial U_{SC} / \partial t = \rho_{YBCO} V_{SC} C_{PYBCO} \partial \bar{T}_{SC} / \partial t \quad (26)$$

where  $\rho_{YBCO}$ ,  $V_{SC}$ , and  $C_{PYBCO}$  are the YBCO density, volume, and specific heat capacity at constant pressure, respectively. According to Equation (26), the thermal power is positive or negative if the bulk average temperature increases or decreases, respectively.

Because of the difficulty in accurately measuring the average bulk temperature evolution, another methodology is proposed to validate experimentally the thermal power released from YBCO bulks during their ZFC. This methodology consists of measuring the LN<sub>2</sub> boiled mass specifically due to the thermal power released from a YBCO bulk. In this second methodology, which is proposed here, the total thermal power associated with LN<sub>2</sub> vaporization by phase change can be determined from the measured evolution of the total LN<sub>2</sub> mass by Equation (27),

$$P_{t \text{ LN}_2} = -L_{\text{LN}_2} \partial M_{\text{LN}_2} / \partial t = -L_{\text{LN}_2} \rho_{\text{LN}_2} \partial V_{\text{LN}_2} / \partial t \quad (27)$$

where  $M_{\text{LN}_2}$  and  $V_{\text{LN}_2}$  are the mass and volume of LN<sub>2</sub>, respectively. The LN<sub>2</sub> latent heat assumes the value  $L_{\text{LN}_2} = 199 \text{ J g}^{-1}$ . According to Equation (27), the increase in the LN<sub>2</sub> evaporated mass results in a negative thermal power value, representing the release of thermal power from the bulk.

The procedure consisted of quickly immersing a bulk with dimensions  $33 \times 33 \times 14 \text{ mm}^3$  at room temperature into the LN<sub>2</sub>, filling the cavity of a box made of extruded polystyrene (XPS) walls. The box's top surface was open to the air. The bulk then stayed immersed in the LN<sub>2</sub> in the middle of the box cavity, suspended on top of four copper rods, each with a 3 mm width. Once the box top surface was open to the air, the temperature step transition occurred at almost constant pressure. In this fast-cooling process, the LN<sub>2</sub> boiling was mainly due to the heat released from the YBCO bulk, in which the heating from room temperature was almost negligible.

A digital scale with 0.1 g resolution was used to measure the evolution of the total system mass symmetric to the evolution of the LN<sub>2</sub> evaporated mass.

The verified bubbling and heat transfer rate was higher near the bulk lateral surface. The bulk lateral surface temperature evolution was measured using a platinum resistor leaning in the middle of this surface, where the predicted thermal power flux was higher. The platinum resistor was oriented vertically from the bottom to the top surfaces. The resistance of this resistor depended on its average temperature  $T$ . The characteristic that gives the temperature as a function of the sensor resistance is expressed by Equation (28).

$$R(T) = R_0 \left( 1 + AT + BT^2 + C(1 - T) T^3 \right) \quad (28)$$

where  $R$  is the measured resistance value ( $\Omega$ ),  $T$  is the corresponding temperature ( $^\circ\text{C}$ ), and  $R_0$  is the resistance value at  $0 \text{ }^\circ\text{C}$  (273 K), assuming a value of  $100 \text{ } \Omega$ . Constants  $A$ ,  $B$ , and  $C$  assume, respectively, values of  $3.908 \times 10^{-3} \text{ }^\circ\text{C}^{-1}$ ,  $-5.775 \times 10^{-7} \text{ }^\circ\text{C}^{-2}$  and  $-4.183 \times 10^{-12} \text{ }^\circ\text{C}^{-3}$ . This characteristic is valid for temperatures  $-200 \text{ }^\circ\text{C} < T < 0 \text{ }^\circ\text{C}$ .

Polyurethane (PUR) shielding was provided to avoid direct contact between the LN<sub>2</sub> and the platinum resistor surface area increasing its sensitivity to the YBCO bulk surface temperature. Figure 2a,b show the frontal and lateral views, respectively, of the used platinum resistor with the provided PUR shielding. Figure 2c shows the assembly of this sensor leaning on the YBCO bulk lateral surface.

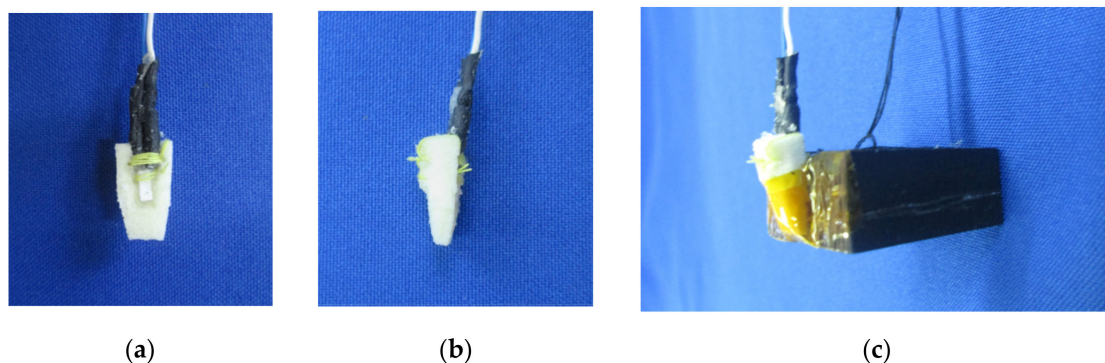


**Figure 2.** Views of the platinum resistor with the PUR shielding on the frontal (a) and lateral (b) directions. The assembly of this sensor leans the YBCO bulk lateral surface (c).

Figure 3a shows the instant before immersing the YBCO bulk into the LN<sub>2</sub> when the box cavity was full of LN<sub>2</sub>. Figure 3b refers to  $t = 60 \text{ s}$  after immersing the bulk when the bulk was already cooled at the LN<sub>2</sub> temperature.

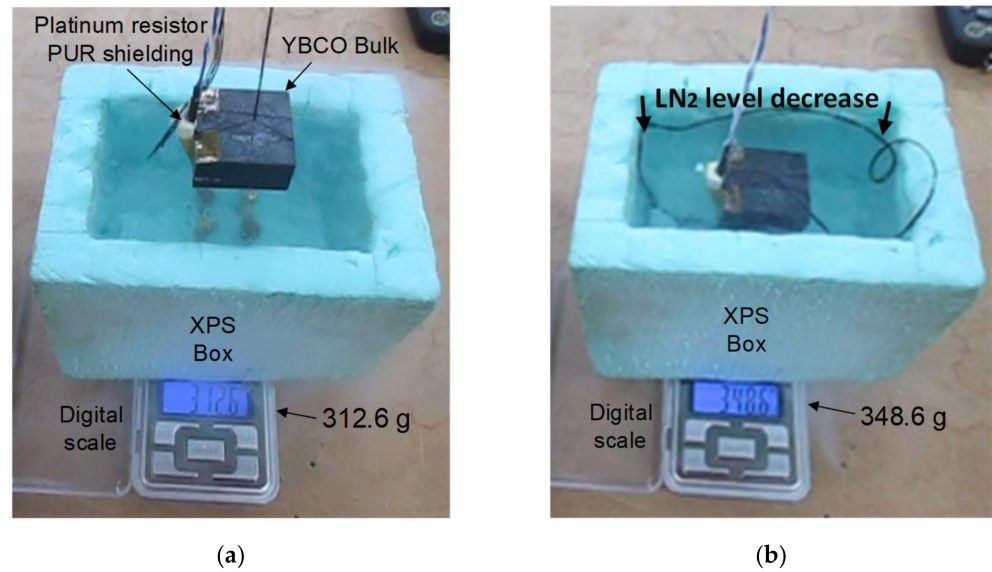


**Figure 3.** The XPS box with LN<sub>2</sub> just before (a) and 60 s after (b) the bulk immersion.

From Figure 3a, related to the instant before immersing the bulk into the LN<sub>2</sub>, one can see the four thin copper rods fixed at the box cavity bottom below the LN<sub>2</sub> level. As one may verify from Figure 3b, the heat released from the YBCO bulk in response to this stepped temperature transition caused LN<sub>2</sub> boiling and the consequent reduction of the LN<sub>2</sub> level. The amount of heat released from the YBCO bulk was determined from the LN<sub>2</sub> evaporated mass, knowing the LN<sub>2</sub> latent heat. This is because, in such a stepped temperature transition, the boiling of LN<sub>2</sub> was mainly due to the heat released from the YBCO bulk, and the effect of LN<sub>2</sub> heating by the room temperature was negligible. The precision of the results is calculated from the rate of LN<sub>2</sub> evaporation due to the room temperature heating with the bulk already cooled by ZFC, which was determined in [12].

#### 4. Analysis of YBCO Temperature and ZFC Thermal Power Release

The total system mass and temperature at the middle of the YBCO bulk lateral surface in response to this environment temperature transition were measured experimentally. Figure 4a–d show the measurements of the total weight and platinum resistance at 0.5, 15, 30, and 60 s after the step transition from the room to LN<sub>2</sub> temperature.

The evolutions of the LN<sub>2</sub> evaporated mass, thermal power released from the YBCO bulk, and its average temperature were predicted using 3D FEA. Because of the existing symmetry, only one-quarter of the full box was simulated using 3D FEA to reduce the associated numerical processing. Figure 5a shows the design with dimensions of one box quarter, and Figure 5b shows the mesh considered in 3D FEA.

In the LN<sub>2</sub> domain, with a constant density of  $808.5 \text{ kg m}^{-3}$ , a moving mesh was adopted. The decreasing volume and height of the LN<sub>2</sub> domain were dependent on the LN<sub>2</sub> mass and box cavity area. The LN<sub>2</sub> mass evaporation rate was dependent on the thermal power released from the YBCO bulk, according to Expression (27). The increasing volume empty of LN<sub>2</sub> was filled with air. A moving mesh was also adopted in this last volume. Heat transfer by natural convection was considered on the external surfaces in contact with the environmental air. The Neumann condition in Equation (15) was considered for the moving boundary between the LN<sub>2</sub> and air volumes. According to Expressions (8) and (9), the considered coefficients of natural convection to the air were  $h_h = 83.58 \text{ Wm}^{-2}\text{K}^{-1}$  on the LN<sub>2</sub> surface and  $h_v = 8.72 \text{ Wm}^{-2}\text{K}^{-1}$  on the vertical XPS wall surfaces.

Figure 6a shows the obtained temperature distribution at  $t = 0.5 \text{ s}$ , when the average temperatures of the YBCO, LN<sub>2</sub>, and XPS domains were close to their initial values. For the initial conditions, a temperature of 293 K was considered for YBCO bulk, platinum resistor, and its foam shielding, and 77 K was considered for the LN<sub>2</sub> and XPS domains. Figure 6b shows the obtained temperature distribution at  $t = 30 \text{ s}$  when the YBCO bulk average temperature was about 110 K. At this time, the level of LN<sub>2</sub> had decreased because of LN<sub>2</sub> boiling, increasing the temperature at the top air level.

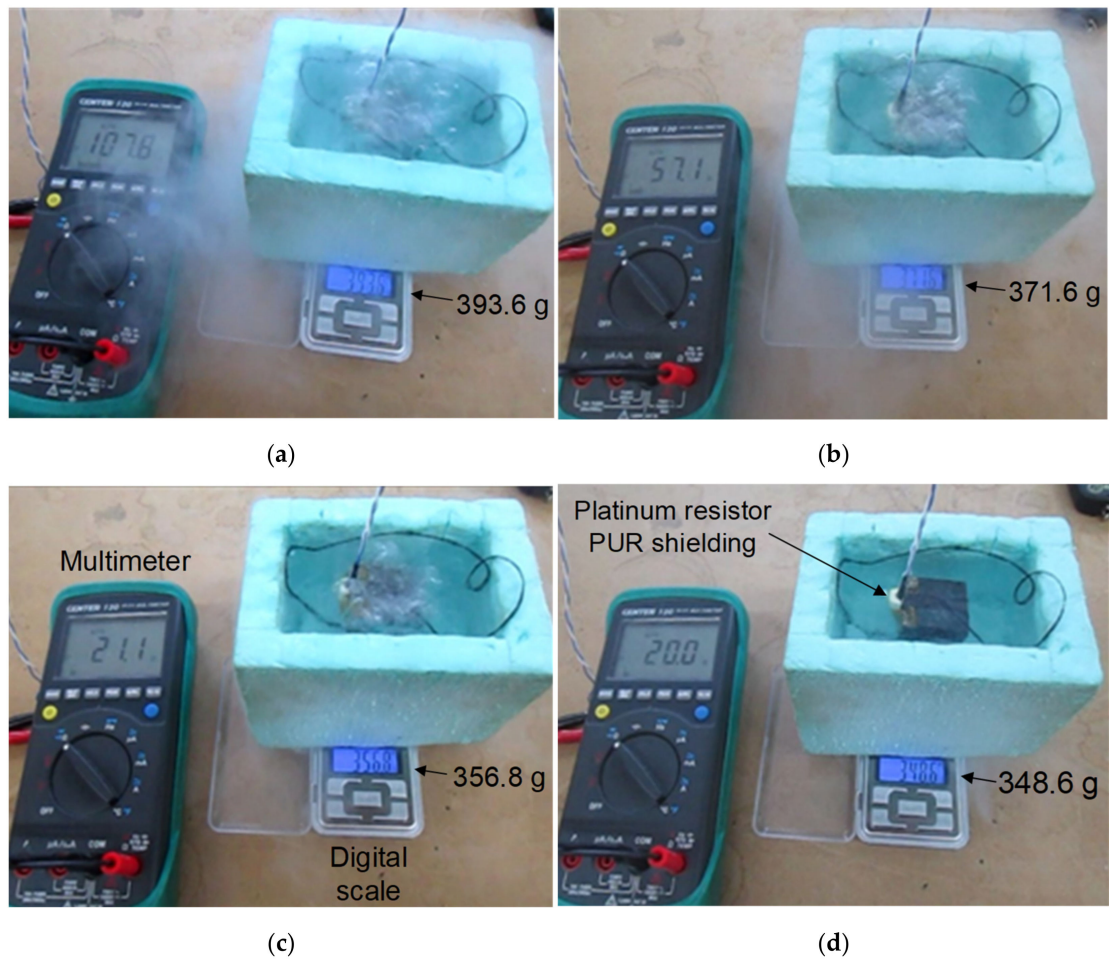


**Figure 4.** Measurements of the total weight and platinum resistance at the instants: (a) 0.5 s, (b) 15 s, (c) 30 s, and (d) 60 s after the step transition from the room to LN<sub>2</sub> temperature.

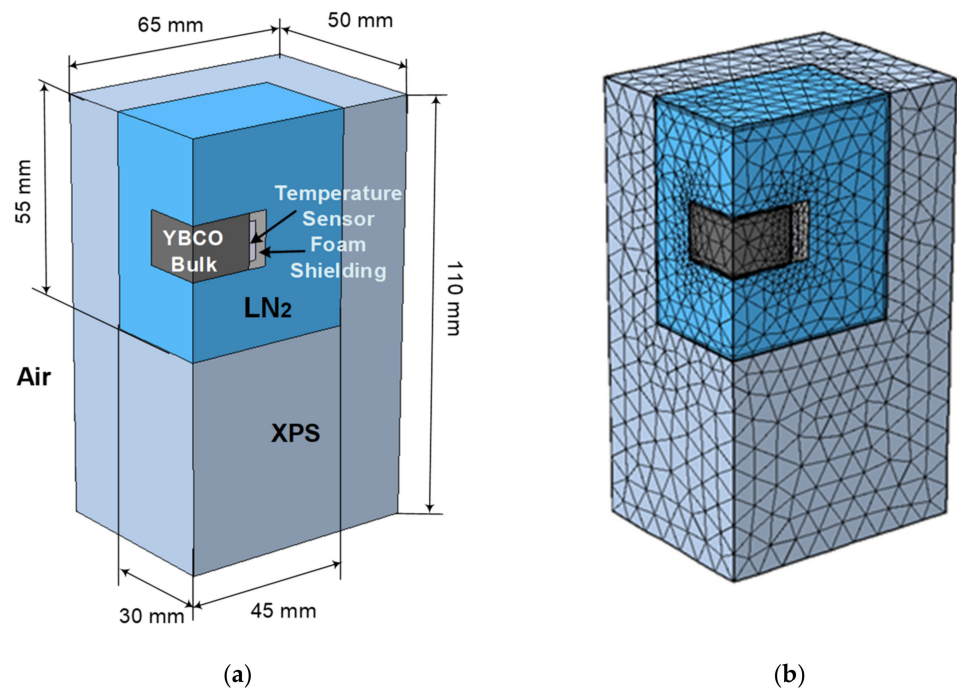


**Figure 5.** Design with dimensions of one box quarter (a) and mesh in 3D FEA (b).

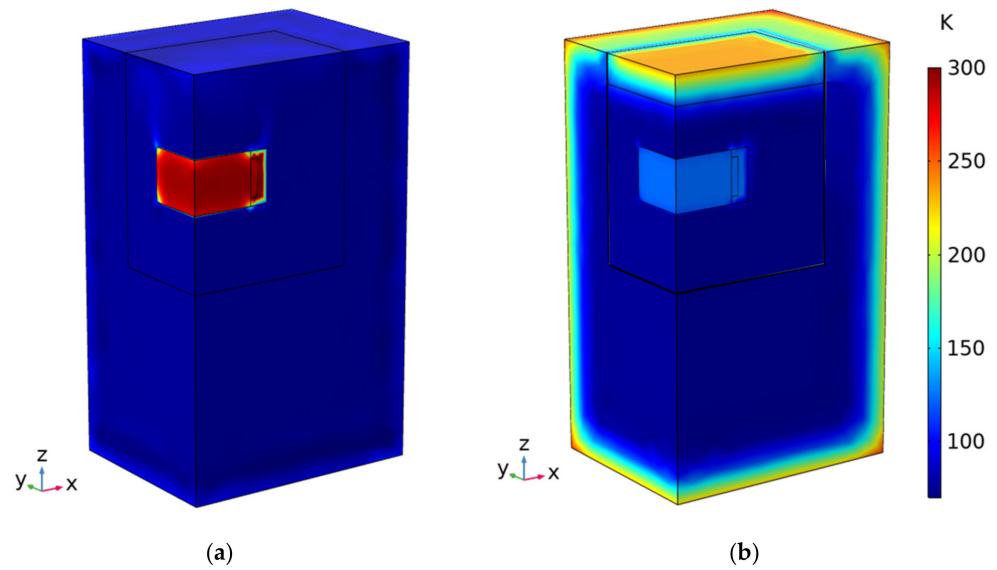


Figure 6. Temperature distribution at (a)  $t = 0.5$  s and (b)  $t = 30$  s.

Figure 7a shows the obtained distribution of the heat flux and LN2 flow velocity streamlines from LN2 boiling at  $t = 0.5$  s, when the generation of bubbles was intense just after the stepped transition. As one may verify, almost all the heat released from the YBCO bulk flew to the top surface open to the air. Figure 7b shows the distribution of heat flux and LN2 flow velocity streamlines at  $t = 30$  s, when the heat release and rate of bubbling had decreased.

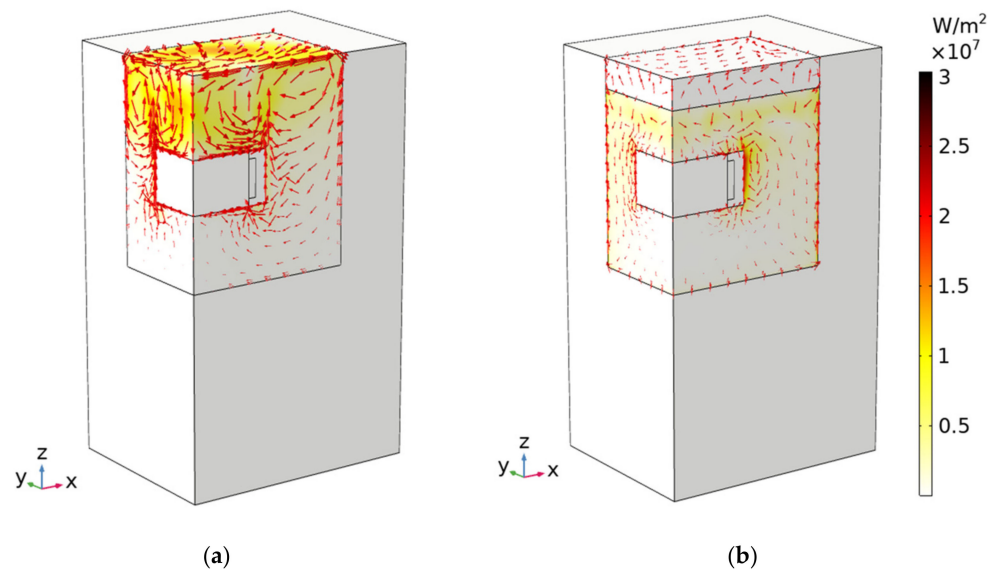


Figure 7. Heat flux distribution and LN2 velocity streamlines at (a)  $t = 0.5$  s and (b)  $t = 30$  s.

Figure 8 relates to the characteristics of the total mass evolution in time. The mass measured using the digital scale is shown as (a), the data obtained through 3D FEA are (b), and those by the exponential fitting of experimental measurements are shown as (c). Figure 9 shows the characteristics of the evolution of thermal power released from the YBCO bulk in time. Characteristic (a) was obtained by discrete analysis of the total mass evolution measured, as shown in characteristic (a) of Figure 8. This discrete analysis consisted of transforming Equation (27) by Equation (29),

$$P_t = -L_{LN2} \partial M_{LN2} / \partial t \Leftrightarrow P_{t_{i+1}} = -L_{LN2} \frac{M_{LN2_{i+1}} - M_{LN2_i}}{t_{i+1} - t_i} \tag{29}$$

where index  $i$  refers to the index at the sampling time  $t_i$ .

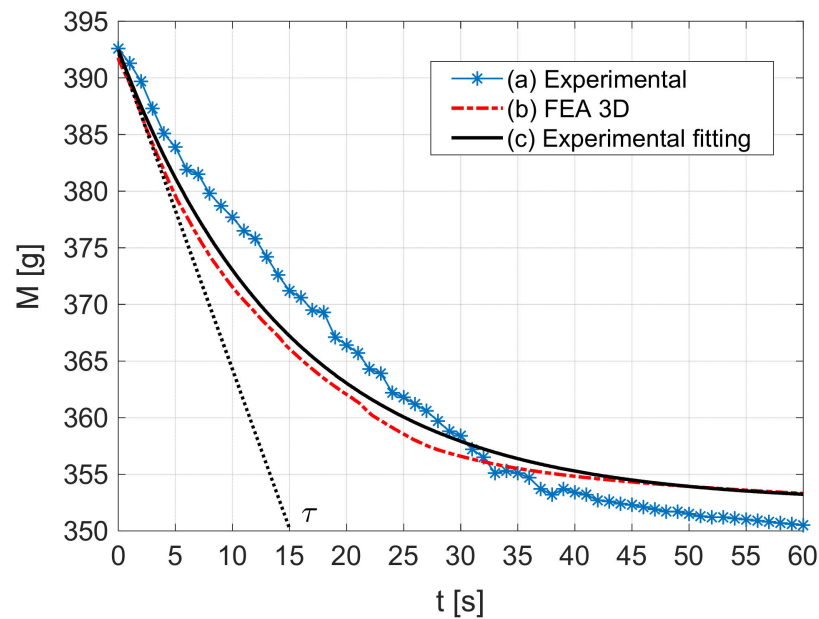


Figure 8. Evolution of the total mass.

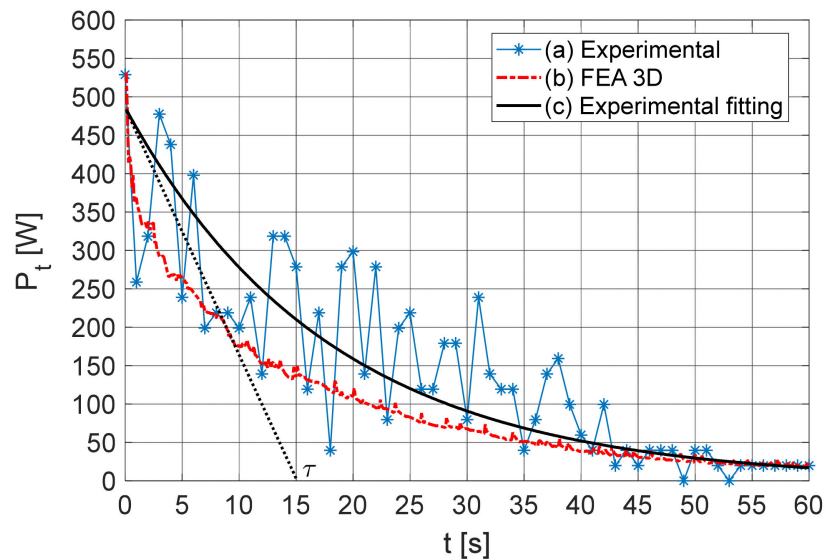


Figure 9. Evolution of thermal power release from the YBCO bulk.

The fluctuations observed in characteristic (a) resulted from small errors in the total mass measurements. Characteristic (b) of Figure 9 refers to the 3D FEA of the heat flux to the LN<sub>2</sub> domain through the boundaries with the YBCO, XPS, and air domains. In this process, the heat flux from the YBCO to LN<sub>2</sub> was almost symmetric to the heat flux from the LN<sub>2</sub> to the air since the heat flux from the LN<sub>2</sub> to the XPS was almost negligible. Characteristic (c) obtained by exponential fitting of characteristic (a).

Figure 10 refers to the evolution of the YBCO bulk temperature in time. Characteristic (a) was obtained by the measurement of the platinum sensor resistance and converted into temperature using Equation (28). Characteristics (b) and (c) resulted from the evaluation of the average temperature of the YBCO bulk and platinum resistor, respectively, obtained through 3D FEA. Characteristic (d) was obtained by the exponential fitting of the measured values from experimental characteristic (a).

During the first 20 s, the average temperature predicted by 3D FEA for the sensor in characteristic (c) did not decay as fast as that predicted for the YBCO bulk in characteristic (b). This effect was because the surfaces of the platinum resistor, which was not leaning the YBCO bulk lateral surface, were shielded by a foam coat to prevent direct contact with the LN<sub>2</sub>. In addition, the YBCO bulk surfaces were directly in contact with the LN<sub>2</sub>, and at the LN<sub>2</sub> boiling temperature, the YBCO

presented a thermal conductivity about 85 times that of LN<sub>2</sub> and 390 times that of XPS foam. This effect was also visible in characteristic (a) obtained experimentally, with a decay in the first 20 s lower than the one predicted by 3D FEA for the YBCO average temperature in characteristic (b).

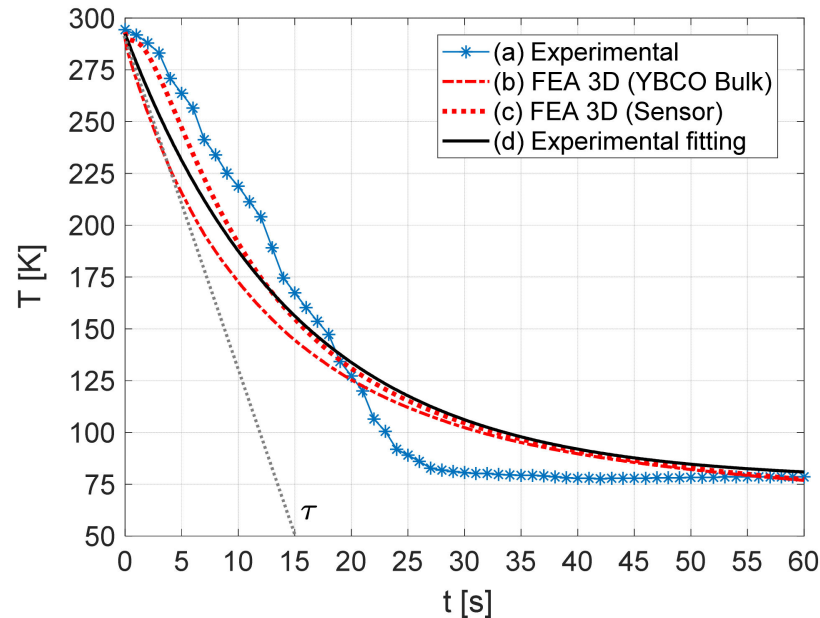


**Figure 10.** Evolution of the YBCO bulk temperature.

In Figures 8–10, the characteristics obtained by the exponential fitting of experimental measurements follow the trends of the ones predicted by 3D FEA, presenting a response time constant of about  $\tau \approx 15$  s. From characteristic (d) of Figure 10, one verifies that the bulk average temperature reached the YBCO critical temperature of superconductivity ( $T_C = 92$  K) at about  $t = 40$  s and the LN<sub>2</sub> average temperature at  $t = 60$  s after the stepped temperature transition.

From characteristic (a) of Figure 8, the measured decay of total mass corresponding to the LN<sub>2</sub> evaporated mass was about  $\Delta M_{LN_2} = -45$  g (i.e.,  $393.6$  g –  $348.6$  g) at 60 s. Multiplying this mass loss by the LN<sub>2</sub> latent heat ( $L_{LN_2} = 199$  J g<sup>-1</sup>) results in a heat release by the YBCO bulk of about  $\Delta Q_{YBCO} = 8.36$  kJ. Almost the same value can be obtained by integrating it with the time characteristic (c) of Figure 9. This corresponds to a bulk average heat capacity at a constant pressure of about  $C_{sc} = Q_{YBCO}/\Delta T \approx 8.36$  kJ/( $293$  K –  $77$  K) =  $38.7$  J K<sup>-1</sup>. Knowing the bulk mass ( $M_{SC} = 90$  g) results in an average specific heat capacity at a constant pressure of about  $C_{PYBCO} = C_{sc}/M_{SC} \approx 430$  J K<sup>-1</sup> kg<sup>-1</sup>.

The same box was considered in [12] to determine the dependence of the average temperature of a YBCO bulk already cooled by ZFC on the LN<sub>2</sub> level. In this study, the rate of LN<sub>2</sub> evaporation due to the heating from room temperature was measured experimentally and validated through 3D FEA. An average rate of  $200$  g h<sup>-1</sup> =  $3.33$  g min<sup>-1</sup> was verified for LN<sub>2</sub> evaporation due to the heating from room temperature. Here, the measured average rate of LN<sub>2</sub> evaporation after this temperature step transition was  $45$  g min<sup>-1</sup>. The expected LN<sub>2</sub> evaporation due only to the thermal power released from the YBCO bulk after 60 s would be  $41.67$  g (i.e.,  $45$  g –  $3.33$  g). Hence, the expected error in the LN<sub>2</sub> evaporated mass was  $\delta \approx (45 - 41.6)/41.6 = 8.2\%$ .

## 5. Validation of YBCO Thermal Parameters from First-Order Step Response Analysis

The YBCO bulk is defined by a heat capacity  $C_{sc}$  and thermal resistance  $R_{sc}$  through the main direction of the heat flux. Hence, a first-order system can modulate its interaction with the environmental temperature. Figure 11 shows the first-order thermal circuit transient that models the considered temperature step transition. The variable  $T$  represents the YBCO bulk average internal temperature, and  $T_e$  is the environment temperature that switches from  $293$  K (room temperature) to  $77$  K (LN<sub>2</sub> average temperature).

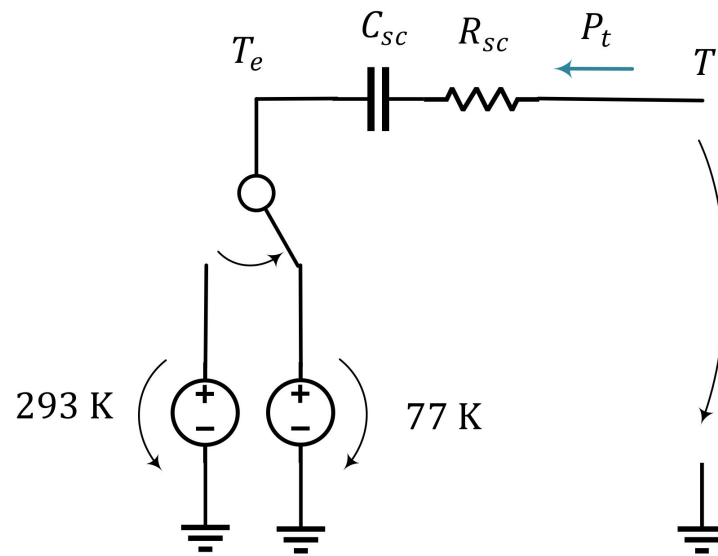


**Figure 11.** The thermal circuit that models the YBCO stepped transition from room to LN<sub>2</sub>.

From the analysis of the circuit results, the differential Equation (30) relates the bulk average internal temperature  $T$  with the thermal power  $P_t$ .

$$T - T_e = R_{sc} P_t + \frac{1}{C_{sc}} \int_0^t P_t dt = R_{sc} \left( P_t + \frac{1}{\tau} \int_0^t P_t dt \right) \tag{30}$$

After the stepped transition,  $T$  decays exponentially to the LN<sub>2</sub> environment average temperature  $T_e = 77$  K, with a time constant  $\tau \approx 15$  s, where the solution is given by Equation (31).

$$T = (293 \text{ K} - 77 \text{ K}) e^{-\frac{t}{\tau}} + 77 \text{ K}; \quad \tau = R_{sc} C_{sc} \approx 15 \text{ s} \tag{31}$$

This solution corresponds to the average of characteristics (b) and (d) of Figure 10. From Equation (30), the dependence of the bulk thermal resistance in the time given by Equation (32) was deduced.

$$R_{sc} = \frac{T - 77 \text{ K}}{\left( P_t + \frac{1}{\tau} \int_0^t P_t dt \right)} \tag{32}$$

The value of  $P_t$  as a function of time was obtained from characteristic (c) of Figure 9. The instantaneous value of the bulk heat capacity  $C_{sc}$  was determined by dividing the first-order response time constant  $\tau \approx 15$  s by the instantaneous value of the bulk thermal resistance  $R_{sc}$ . The characteristics of dependence on temperature,  $R_{sc}(T)$  and  $C_{sc}(T)$ , were obtained by correlating the obtained characteristics of dependence with time,  $R_{sc}(t)$  and  $C_{sc}(t)$ , with the dependence of the bulk average temperature in time expressed by Equation (31). Figure 12 shows the obtained characteristics of dependence of the YBCO bulk heat capacity and thermal resistance from its internal average temperature,  $R_{sc}(T)$  and  $C_{sc}(T)$ .

The characteristic of dependence on temperature of the YBCO thermal conductivity  $k_{YBCO}(T)$  is obtained using Equation (33).

$$k_{YBCO}(T) = \frac{L}{R_{sc}(T) S} \tag{33}$$

where  $L$  and  $S$  represent the bulk equivalent length and surface area through the main direction of the heat flux, respectively. To reduce the analytical complexity of the problem, the bulk is assumed as a sphere of the same volume  $V_{SC} = 33 \times 33 \times 14 \text{ mm}^3 = 15.25 \text{ cm}^3$  with omnidirectional heat flux. The sphere is defined by a radius  $r = \sqrt[3]{3V_{SC}/(4\pi)} = 15.38 \text{ mm}$  and surface area  $S = 4\pi r^2 = 29.72 \text{ cm}^2$ . Dimension  $L$  is given by the relationship between the bulk volume and its surface area, resulting  $L = 5.13 \text{ mm}$ .

The characteristic of dependence on temperature of the YBCO specific heat capacity at constant pressure  $C_{pYBCO}(T)$  was obtained by Equation (34).

$$C_{pYBCO}(T) = \frac{C_{sc}(T)}{\rho_{YBCO} V_{SC}} \tag{34}$$

where  $V_{SC}$  is the bulk volume and  $\rho_{YBCO} = 5900 \text{ kg m}^{-3}$  is the YBCO density.

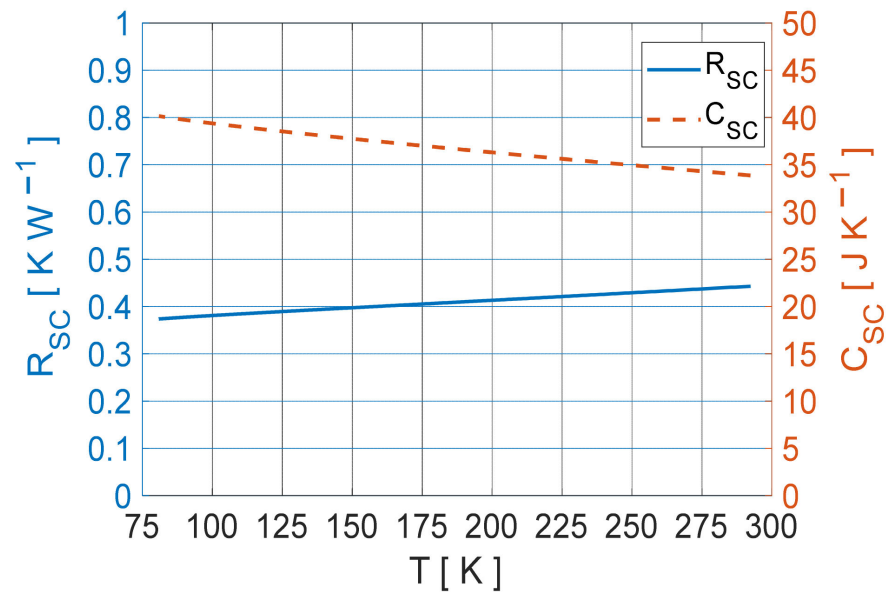


Figure 12. YBCO bulk heat capacity and thermal resistance dependence from internal temperature.

Conventional and oscillatory thermal response tests (TRTs) to determine the thermal conductivity and heat capacity of a subsurface were performed [30].

Figure 13 compares the obtained characteristics of dependence on temperature of the YBCO thermal conductivity and specific heat capacity at constant pressure,  $k_{YBCO}(T)$  and  $C_{pYBCO}(T)$ , with the ones in the literature [16–19], as stated in Section 2.1.

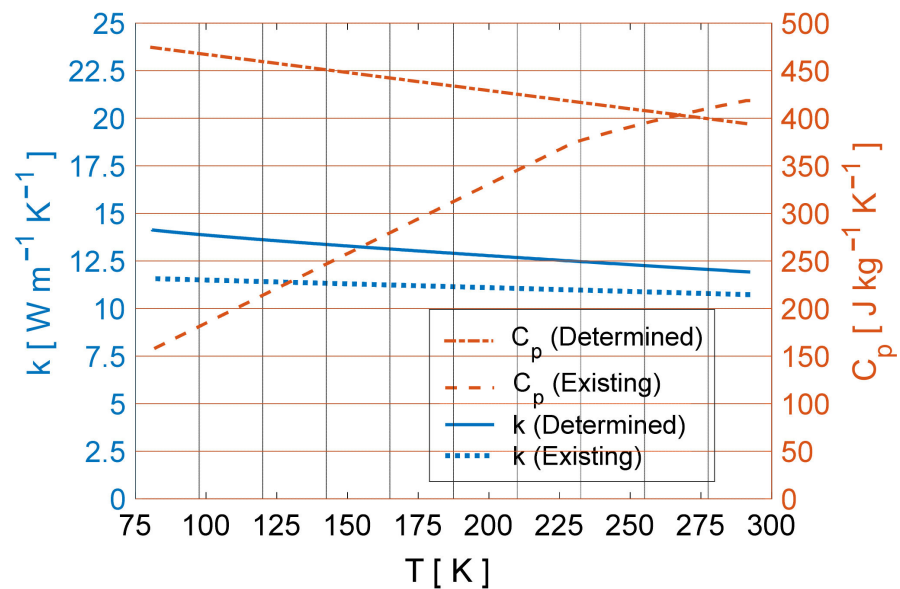


Figure 13. Dependence of YBCO thermal conductivity and specific heat capacity with temperature.

The obtained characteristic of YBCO specific heat capacity at constant pressure (dashed-dotted brown line) presents an average value approximately equal to the one calculated in the final part of Section 4 ( $C_{PYBCO} \approx 430 \text{ J K}^{-1} \text{ kg}^{-1}$ ). Contrary to the characteristic in the literature for the YBCO layer in stacked tapes and coated conductors [19,20] (dashed brown line), the trend of the obtained characteristic for  $C_{PYBCO}(T)$  decreases with temperature. This makes sense because the higher the bulk temperature, the less its capacity to absorb heat. This characteristic assumes values of the same order that are approximately equal to the ones found in the literature for temperatures around 260 K.

The obtained characteristic of YBCO thermal conductivity (continuous blue line) closely follows the existing one found in the literature [16–18] (dotted blue line). Their trends indicate a decrease in YBCO thermal conductivity with temperature.

## 6. Conclusions

This study presents results from a simple experimental methodology that may be used to determine with expected precision the heat released by a YBCO bulk during its zero-field cooling (ZFC). This amount of heat is associated with the total thermal energy in the bulk mass and is independent of the cooling time. The adopted methodology consisted in determining this amount of heat from the LN<sub>2</sub> consumption after a stepped transition of the YBCO from room to the LN<sub>2</sub> temperature by a quick immersion of the bulk into LN<sub>2</sub>. Although the cooling of YBCO bulks should be progressive, this fast-step cooling process was adopted to minimize the amount of LN<sub>2</sub> evaporation by the influence of room temperature heating with relation to the amount of LN<sub>2</sub> evaporation due to the heat released from the YBCO bulk. The precision of the results was calculated from the average rate of LN<sub>2</sub> evaporation due to the room temperature heating with the bulk already cooled by ZFC, which was measured previously.

The evolutions of the bulk average temperature and thermal power release over time presented typical first-order step responses with the time constant  $\tau \approx 15$  s. According to the experimental measurements, about 45 g of LN<sub>2</sub> evaporated after the quick immersion of a YBCO bulk with dimensions  $33 \times 33 \times 14$  mm<sup>3</sup> at room temperature into LN<sub>2</sub>. Considering the LN<sub>2</sub> latent heat, this produced 8.36 kJ of heat. The expected LN<sub>2</sub> mass evaporated in excess due to the heat from room temperature was about 3.33 g, which corresponds to an error of +8.2%. Thus, about 41.7 g of LN<sub>2</sub> evaporation was due to the heat released from a YBCO bulk. Hence, the expected heat released from the YBCO bulk during ZFC was effectively 8.3 kJ. Dividing this heat by the change in the bulk temperature of about 216 K (i.e., 293 K – 77 K) results in an average value for the YBCO heat capacity of 38.7 J K<sup>-1</sup>. Dividing this value by the bulk's mass equal to 90 g results in an average value for the YBCO-specific heat capacity at a constant pressure of about 430 J K<sup>-1</sup> kg<sup>-1</sup>, which corresponds to the value in the literature for the YBCO-specific heat at constant pressure at the temperature of 77 K (LN<sub>2</sub> boiling temperature).

From the evolutions of the bulk average temperature and thermal power release over time, the bulk heat capacity and thermal resistance were determined. The characteristics of dependence on temperature of the bulk heat capacity and thermal resistance were obtained by correlating the corresponding evolutions over time with the obtained dependence of the bulk internal temperature with time. From these, the characteristics of dependence on temperature of the YBCO thermal conductivity and specific heat at constant pressure were calculated, which follow closely to the ones found in the literature.

**Author Contributions:** Conceptualization, A.J.A.C., J.F.P.F., R.M., C.C. and P.J.C.B.; methodology, A.J.A.C., J.F.P.F. and P.J.C.B.; software, A.J.A.C. and J.F.P.F.; validation, R.M., C.C. and P.J.C.B.; formal analysis, A.J.A.C., J.F.P.F. and P.J.C.B.; investigation, A.J.A.C. and J.F.P.F.; resources, R.M., C.C. and P.J.C.B.; writing—original draft preparation, A.J.A.C.; writing—review and editing, A.J.A.C., J.F.P.F., R.M., C.C. and P.J.C.B.; supervision, R.M., C.C. and P.J.C.B.; Project administration, P.J.C.B.; Funding acquisition, P.J.C.B. All authors have read and agreed to the published version of the manuscript.

**Funding:** This research received no external funding.

**Institutional Review Board Statement:** Not applicable.

**Informed Consent Statement:** Not applicable.

**Data Availability Statement:** Not applicable.

**Acknowledgments:** This work was supported by Fundação para a Ciência e Tecnologia (FCT), through IDMEC, under LAETA, project UIDB/50022/2020. To previous research supported by FCT project PTDC/EEEIEEL/4693/2014—HTSISTELEC and FCT fellowship SFRH/BD/117921/2016.

**Conflicts of Interest:** The authors declare no conflict of interest.

## Nomenclature

### Acronyms

ZFC	Zero-field cooling
YBCO	Yttrium barium copper oxide
XPS	Extruded polystyrene
PUR	Polyurethane
LN <sub>2</sub>	Liquid nitrogen
FEA	Finite element analysis
TRT	Thermal response test

### Symbols

$T$	Temperature
$u$	Velocity
$p$	Pressure
$\rho$	Volumetric density
$k$	Thermal conductivity
$k_{YBCO}$	YBCO thermal conductivity
$k_{LN_2}$	LN <sub>2</sub> thermal conductivity
$C_p$	Specific heat capacity at constant pressure
$C_{pYBCO}$	YBCO-specific heat capacity at a constant pressure
$C_{pLN_2}$	LN <sub>2</sub> specific heat capacity at a constant pressure
$Q$	Heating source volumetric power density
$q$	Thermal power flux
$q_e$	Thermal power flux by natural convection to environmental air
$h$	Convection coefficient
$h_h$	Convection coefficient through a horizontal surface
$h_v$	Convection coefficient through a vertical surface
$T_e$	External environmental temperature
$L_{LN_2}$	LN <sub>2</sub> latent heat
$R_a$	Rayleigh number
$\Phi_{mLN_2}$	Rate of LN <sub>2</sub> evaporated mass flux
$Re$	Reynolds number
$\mu$	Fluid dynamic viscosity
$\mu_{LN_2}$	LN <sub>2</sub> dynamic viscosity
$\mu_{air}$	Dynamic viscosity of the air
$\nu$	Fluid kinetic viscosity
$\kappa$	Turbulent kinetic energy
$\varepsilon$	Rate of dissipation of turbulent energy
$\mu_t$	Turbulent or eddy viscosity
$P_k$	Rate of production of turbulent kinetic energy
$U_{SC}$	Superconductor bulk internal energy
$\overline{T}_{SC}$	Superconductor bulk average temperature
$V_{SC}$	Superconductor bulk volume
$V_{LN_2}$	LN <sub>2</sub> domain volume
$M_{LN_2}$	LN <sub>2</sub> domain mass
$P_t$	Thermal power
$R_{sc}$	Bulk equivalent thermal resistance in the main direction of heat flux
$C_{sc}$	Superconductor bulk heat capacity
$\tau$	Time constant
$\delta$	Error in LN <sub>2</sub> evaporated mass

## References

1. Xiao, L.; Ren, H.T.; Jiao, Y.L.; Zheng, M.H.; Chen, Y.X. Effects of cooling rate on single domain growth and the superconducting properties for YBCO bulk. *Phys. C* **2003**, *386*, 262–265. [[CrossRef](#)]
2. Ceniga, L.; Diko, P. Matrix crack formation in Y–Ba–Cu–O superconductor. *Phys. C* **2003**, *385*, 329–336. [[CrossRef](#)]
3. Diko, P.; Krabbes, G. Formation of c-macrocracks during oxygenation of TSMG YBa<sub>2</sub>Cu<sub>3</sub>O<sub>7</sub>/Y<sub>2</sub>BaCuO<sub>5</sub> single-grain superconductors. *Phys. C* **2003**, *399*, 151–157. [[CrossRef](#)]
4. Floegel-Delor, U.; Schirrmeister, P.; Riedel, T.; Koenig, R.; Kantarbar, V.; Werfel, F.N. Bulk Superconductor Levitation Devices: Advances in and Prospects for Development. *IEEE Trans. Appl. Supercond.* **2018**, *28*, 1–5. [[CrossRef](#)]

5. Dias, D.H.N.; Sotelo, G.G.; Sass, F.; Motta, E.S.; de Andrade, R., Jr.; Stephan, R.M. Dynamical tests in a linear superconducting magnetic bearing. *Phys. Procedia* **2012**, *36*, 1049–1054. [[CrossRef](#)]
6. Sotelo, G.G.; de Andrade, R., Jr.; Dias, D.H.N.; Ferreira, A.C.; Costa, F.; Machado, O.J.; de Oliveira, R.A.H.; Santos, M.D.A.; Stephan, R.M. Tests With One Module of the Brazilian Maglev-Cobra Vehicle. *IEEE Trans. Appl. Supercond.* **2013**, *23*, 3601204. [[CrossRef](#)]
7. Werfel, F.N.; Floegel-Delor, U.; Rothfeld, R.; Riedel, T.; Schirrmeister, P.; Koenig, R. Experiments of Superconducting Maglev Ground Transportation. *IEEE Trans. Appl. Supercond.* **2016**, *26*, 1–5. [[CrossRef](#)]
8. Zheng, J.; Li, J.; Sun, R.; Qian, N.; Deng, Z. A magnetic levitation rotating plate model based on high-Tc superconducting technology. *Cryogenics* **2017**, *86*, 1–6. [[CrossRef](#)]
9. Zhang, S.; Ren, Y.; Du, Y.; Zheng, J.; Deng, Z. Dynamic Liquid Nitrogen Level Detection of Cryostats On board the HTS MagLev Vehicle. *IEEE Trans. Appl. Supercond.* **2019**, *28*, 1–5.
10. Wen, P.; Wang, W.; Ren, Y.; Lei, W.; Chen, H.; Xua, Y.; Deng, Z. Design and Implementation of auto-filling liquid nitrogen for HTS maglev vehicles based on Kalman filter algorithm. *Cryogenics* **2020**, *111*, 103167. [[CrossRef](#)]
11. Arsénio, A.J.; Melicio, R.; Carneira, C.; Costa Branco, P.J. The Critic Liquid–Gas Phase Transition Between Liquid Nitrogen and YBCO HTS Bulks: From FEM Modeling to its Experimental Study for ZFC Levitation Devices. *IEEE Trans. Appl. Supercond.* **2018**, *28*, 1–8. [[CrossRef](#)]
12. Costa Arsénio, A.J.; Costa Branco, P.J. Thermo-Hydraulic Analysis of a Horizontal HTS ZFC Levitating Bearing Concerning Its Autonomy Safety Service Time. *IEEE Trans. Appl. Supercond.* **2021**, *31*, 1–10. [[CrossRef](#)]
13. Arsénio, A.J.; Silva, F.F.; Fernandes, J.F.P.; Costa Branco, P.J. Optimization of the Guiding Stability of a Horizontal Axis HTS ZFC Radial Levitation Bearing. *Actuators* **2021**, *10*, 311. [[CrossRef](#)]
14. Holman, J.P. *Heat Transfer*, 10th ed.; McGraw-Hill: New York, NY, USA, 2010; ISBN 978-0-07-352936-3.
15. Incropera, F.P.; Dewitt, D.P.; Bergman, T.L.; Lavine, A.S. *Fundamentals of Heat and Mass Transfer*, 6th ed.; John Wiley & Sons: Hoboken, NJ, USA, 2007; ISBN 9780471457282.
16. Ikebe, M.; Fujishiro, H.; Naito, T.; Noto, K.; Kohayashi, S.; Yoshizawa, S. Thermal conductivity of YBCO(123) and YBCO(211) mixed crystals prepared by MMTG. *Cryogenics* **1994**, *34*, 57–61. [[CrossRef](#)]
17. Fujishiro, H.; Ikebe, M.; Naito, T.; Noto, K.; Kohayashi, S.; Yoshizawa, S. Anisotropic Thermal Diffusivity and Conductivity of YBCO(123) and YBCO(211) Mixed Crystals. *Jpn. J. Appl. Phys.* **1994**, *33*, 6157–6159. [[CrossRef](#)]
18. Zhang, M.; Matsuda, K.; Coombs, T.A. New application of temperature-dependent modelling of high temperature superconductors: Quench propagation and pulse magnetization. *J. Appl. Phys.* **2012**, *112*, 043912. [[CrossRef](#)]
19. Feng, J. *Thermohydraulic-Quenching Simulation for Superconducting Magnets Made of YBCO HTS Tape*; Plasma Science and Fusion Center—Massachusetts Institute of Technology Cambridge: Cambridge, MA, USA, 2010; PSFC/RR-10-7.
20. Bae, J.H.; Park, H.Y.; Eom, B.Y.; Seong, K.C.; Baik, S.K. Thermal stability of YBCO coated conductor with different Cu stabilizer thickness. *Phys. C* **2010**, *470*, 1880–1882. [[CrossRef](#)]
21. Placido, E.; Arduini-Schuster, M.; Kuhn, J. Thermal properties predictive model for insulating foams. *Infrared Phys. Technol.* **2005**, *46*, 219–231. [[CrossRef](#)]
22. Abdou, A.; Budaiwi, I. Comparison of thermal conductivity measurements of building insulation materials under various operating temperatures. *J. Build. Phys.* **2005**, *29*, 171–184. [[CrossRef](#)]
23. Perkins, R.A.; Roder, H.M.; Friend, D.G. The thermal conductivity and heat capacity of fluid nitrogen. *Phys. A* **1991**, *173*, 332–362. [[CrossRef](#)]
24. Stephan, K.; Krauss, R. Viscosity and thermal conductivity of nitrogen for a wide range of fluid states. *J. Phys. Chem.* **1987**, *16*, 1–32. [[CrossRef](#)]
25. Jacobsen, R.T.; Stewart, R.B. Thermodynamic Properties of Nitrogen Including Liquid and Vapor Phases from 63 K to 2000 K with Pressures to 10,000 Bar. *J. Phys. Chem. Ref. Data* **1973**, *2*, 757–922. [[CrossRef](#)]
26. Lemmon, E.W.; Jacobsen, R.T. Viscosity and thermal conductivity equations for nitrogen, oxygen, argon, and air. *Int. J. Thermophys.* **2004**, *25*, 21–69. [[CrossRef](#)]
27. Spurk, J.H.; Aksel, N. *Fluid Mechanics*, 2nd ed.; Springer: Berlin/Heidelberg, Germany, 2008; ISBN 978-3-540-73536-6.
28. Munson, B.R.; Young, D.F.; Okiishi, T.H.; Huebsch, W.W. *Fundamentals of Fluid Mechanics*, 6th ed.; Wiley: New York, NY, USA, 2009; ISBN 978-0470-26284-9.
29. Lopez de Bertodano, M.; Lahey, R.T.; Jones, C., Jr. Development of a k-ε Model for Bubbly Two-Phase Flow. *Trans. Am. Soc. Mech. Eng.* **1994**, *116*, 128–134. [[CrossRef](#)]
30. Giordano, N.; Lamarche, L.; Raymond, J. Evaluation of Subsurface Heat Capacity through Oscillatory Thermal Response Tests. *Energies* **2021**, *14*, 5791. [[CrossRef](#)]

**Disclaimer/Publisher’s Note:** The statements, opinions and data contained in all publications are solely those of the individual author(s) and contributor(s) and not of MDPI and/or the editor(s). MDPI and/or the editor(s) disclaim responsibility for any injury to people or property resulting from any ideas, methods, instructions or products referred to in the content.